

Red Supergiant Stars within the Local Group

Lee. R. Patrick



Doctor of Philosophy
The University of Edinburgh
March 2016

Chapter 1

First steps outside the Local Group of Galaxies: Red Supergiants in NGC 55

1.1 Opening remarks

Owen has kindly helped reconstruct and combine the data sets

1.2 Introduction

NGC 55 is a galaxy located outside of the Local Group of Galaxies within the Sculptor Group at a distance of 1.94 ± 0.03 Mpc (Pietrzyński et al., 2006; Gieren et al., 2008) which, before the emergence of the Araucaria Project (Gieren et al., 2005), had been subject to considerable uncertainty (e.g. Pritchett et al., 1987; van de Steene et al., 2006).

The Sculptor Group is considered to be the closest group of galaxies to our own and offers a fantastic laboratory with which to test theories of stellar and galactic evolution as using an 8-m class telescope, one can resolve individual stars within this group. Association to the Sculptor group however, is a contentious issue. Distance estimates vary to each galaxy, but typically when one references this group the main galaxies associated to this reference are: NGC 55, NGC 247,

NGC 253, NGC 300 and NGC 7793. Where NGC 253 is a large starburst galaxy which is the brightest and most dominant galaxy within this group. In addition to these five large spiral galaxies, there are also numerous (~ 20) dwarf galaxies associated to this group.

By revising distances for nine of these dwarfs Karachentsev et al. (2003) postulated that the Sculptor group was actually more like a filament of galaxies, which intersects the Milky Way group, where NGC 55 and NGC 300 and their surrounding satellite galaxies were potentially not associated with the main group of galaxies in this filament. Regardless of the geometry and association to the Sculptor Group, NGC 55 is the nearest large galaxy to the MW group in the direction of the Sculptor Group.

The morphology of NGC 55 is asymmetric and complicated owing to the high inclination angle (up to 80° ; Hummel, Dettmar & Wielebinski, 1986; Westmeier, Koribalski & Braun, 2013). de Vaucouleurs (1961) classified this galaxy as an LMC-like spiral barred galaxy (SB(s)m) where the bar is seen along the line of sight de Vaucouleurs (1961) prompting various claims that this galaxy is an edge on analogue of the LMC (e.g. Robinson & van Damme, 1964, although not cited heavily – two citations in 50 years – the idea has propagated). Figure 1.1 shows NGC 55 and its complicated morphology where one can see the edge-on disk along the major axis of the galaxy and the brighter central part of the galaxy represents the head of the bar. In addition, to NGC 55 being orientated nearly edge on, extending from the disk-bar system there exists many star formation features such as giant H II regions as well as supergiant filaments and shells which are thought to allow ionising radiation to be transported to the halo where star-formation is currently occurring (Ferguson, Wyse & Gallagher, 1996).

The morphology of NGC 55, as well as its known population of massive hot stars (Castro et al., 2008, 2012), points to a recent history of intense star formation. This is supported by the infrared morphology of NGC 55 which is dominated by young star forming features (Engelbracht et al., 2004, with a star formation rate of $0.22 \text{ M}_\odot \text{yr}^{-1}$) as well as indications from near-IR imaging (Davidge, 2005).

The metal content of NGC 55 is expected to be LMC-like, which is supported by Castro et al. (2012) who measured metallicities of 12 blue supergiants using optical spectroscopy and found a mean metallicity $[Z] = -0.40 \pm 0.13 \text{ dex}$. In addition, Webster & Smith (1983) measure abundances of seven H II regions across



Figure 1.1 *Image of NGC 55 where the edge on disk of the galaxy makes up the major axis and the bright central region represents the head of the bar containing intense star forming regions. Image from the Wide Field Imager on the 2.2-metre MPG/ESO telescope at ESO La Silla Observatory. Credit: ESO, press release.*

the disk of NGC 55 using the strong-line method (as well as four measurements of the auroral “direct” line method) and found a similar LMC-like metallicity.

Even though the hot massive star population of NGC 55 has been explored, there currently exists no confirmed RSGs in NGC 55, although Davidge (2005) note that the near-IR CMDs of fields within the disk of NGC 55 reveal signatures of RSGs. This study represents the first quantitative study of RSGs in NGC 55 and, by measuring metallicities of this population, will provide a crucial test of the metallicity gradient within this galaxy.

In this chapter I describe the observations undertaken in Section 1.3 and highlight the target selection method and its uncertainties. Section 1.4 details the data reduction process and its complications owing to the poor S/N ratios of the observations. I then present the main results of the chapter in Section 1.5 where I first measure radial velocities for each epoch of the RGSs, confirming their membership to NGC 55, and then go on to measure stellar parameters for each target using the *J*-band analysis technique described in detail in Chapter ???. Section 1.6 presents a discussion of the results and the main conclusions are presented in Section 1.7.

1.3 Observations

The observations for this study were taken using three nights of KMOS guaranteed time observations (GTO) containing xx RSG candidates, the first of which was taken in October 2013 as part of the observations which led to the publication of Gazak et al. (2015). These data consisted of six science exposures (S) of 600s with sky offset exposures (S) interleaved in an O, S, O observing pattern. Seeing conditions for these data were good at $0''.8$ – $1''.2$ throughout the course of the observing block (OB).

The second data set which is made use of in this chapter comes from two nights in September 2014 where the OB used in 2013 was used as backup observations for a programme which required excellent seeing ($< 0''.6$). The seeing limits on our observations are more relaxed ($< 1''.5$) which gave us an opportunity to make use of some slightly poorer quality KMOS data. On the first night in September 2014 where this OB was observed, the seeing conditions varied widely ($> 1''.6$) prompting one observer to comment that “this is the worst recorded seeing at Paranal!”. However, there are 24 science exposures where the seeing conditions were better than $2''.2$, which are (potentially) useful. The final night of observing consisted of 12 exposures with seeing conditions varying between $1''.1$ – $1''.6$.

In addition to the science exposures obtained, on each night a standard set of KMOS calibration files were obtained as well as standard star observations on each night. The standard star observing block for each night is slightly different where in October 2013 HIP 3820 (B8 V; Houk, 1978) was observed using the 24-arm telluric template (KMOS_spec_acq_stdstarscipatt). However, in September 2014 only the three-arm telluric template was observed (KMOS_spec_cal_stdstar), this time with HIP 18926 (B3 V; Houk & Smith-Moore, 1988) and HIP 3820 on both nights.

interestingly both with radial velocity measurements. Could do some nice calibration of the RV measurements? or update their measurements ... remember, we've chosen them to be featureless in this region

Table 1.1 shows the mean measured resolution and resolving power, at the appropriate rotator angles, for each night where the NGC 55 data were taken. This table shows that the resolution can vary significant between each night,

Table 1.1 Measured velocity resolution and resolving power across each detector.

Date	Det.	IFUs	Ne $\lambda 1.17700 \mu\text{m}$		Ar $\lambda 1.21430 \mu\text{m}$	
			FWHM (km s $^{-1}$)	R	FWHM (km s $^{-1}$)	R
14-10-2013	1	1-8	95.48 \pm 2.42	3140 \pm 80	90.71 \pm 2.09	3305 \pm 76
	2	9-16	88.67 \pm 1.67	3381 \pm 64	86.35 \pm 1.84	3472 \pm 74
	3	17-24	82.89 \pm 1.81	3617 \pm 79	80.56 \pm 2.11	3721 \pm 97
16-10-2013	1	1-8	95.48 \pm 2.46	3140 \pm 81	90.78 \pm 2.12	3302 \pm 77
	2	9-16	88.91 \pm 1.66	3371 \pm 63	86.30 \pm 1.85	3473 \pm 74
	3	17-24	82.96 \pm 2.14	3612 \pm 76	80.77 \pm 2.14	3712 \pm 98
14-09-2015	1	1-8	84.18 \pm 1.93	3561 \pm 82	81.76 \pm 2.15	3667 \pm 96
	2	9-16	87.00 \pm 1.69	3446 \pm 67	84.67 \pm 1.93	3541 \pm 81
	3	17-24	97.14 \pm 1.88	3086 \pm 60	94.85 \pm 2.01	3161 \pm 67
15-09-2014	1	1-8	82.55 \pm 1.96	3632 \pm 86	80.41 \pm 2.30	3728 \pm 106
	2	9-16	88.08 \pm 1.78	3404 \pm 69	86.03 \pm 1.96	3485 \pm 80
	3	17-24	98.04 \pm 1.91	3058 \pm 59	96.74 \pm 2.05	3099 \pm 66

particularly on detector three where the mean resolving power changes by a factor of 1/5.

1.3.1 Target Selection

In order to select RSG candidates in NGC 55 I compiled optical photometry from two sources: The Araucaria Project (Gieren et al., 2005) and the ACS Nearby Galaxy Survey Treasury project (ANGST Dalcanton et al., 2009). Figure 1.2 displays the footprints of the two projects.

- Describe the two projects and their limitations:
- Araucaria: Wide field ground-based with the aim of measuring distances using Cephieds and BSGs
- ANGST: deeper HST survey of nearby (≈ 4 Mpc) galaxies covering some of the disk in NGC 55.
- Selected based on cuts in the ANGST photometry and then applied to the ground based survey

Targets were selected based on the optical photometry from the Araucaria Project (Gieren et al., 2005). The optical CMD which is used to select targets is

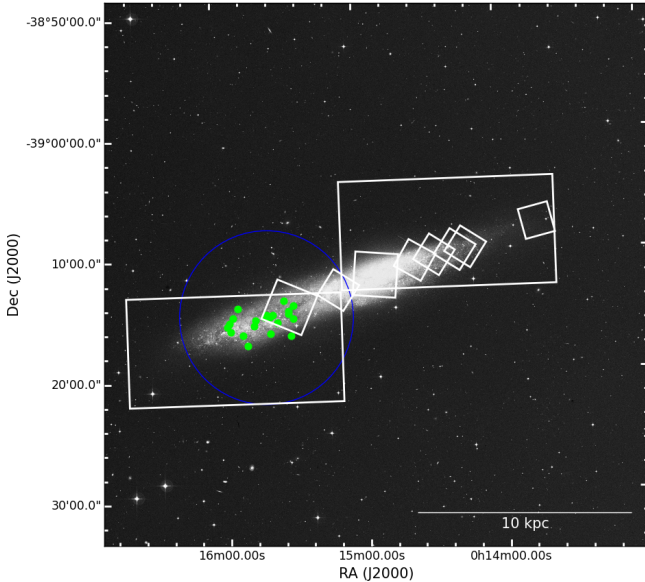


Figure 1.2 DSS image of NGC 55 with KMOS targets overlaid in green and photometric footprints from the Araucaria Project (Gieren et al., 2005) in white rectangles and the ANGST project (Dalcanton et al., 2009) in the smaller white squares.

displayed in Figure ??, where the RSG candidates are within the grey box and the observed targets are highlighted in red. This method of target selection was chosen based on the limited extent of near-IR photometry in this area. Figure ?? displays the footprints from the Araucaria Project (green) and the ACS Nearby Galaxy Survey Treasury (blue; ANGST Dalcanton et al., 2009) in NGC 55 overlaid on a — image.

The selection criteria employed in this study makes use of the optical $V - I$ colours and m_I magnitudes. Owing to their cool temperatures and extreme luminosities RSGs are known to exist in a “plume” at the tip of a structure of cool stars in the $V - I, m_I$ CMD (?) Figure ?? displays this CMD and the region of parameter space where RSG candidates reside is marked with a grey box. This box has the limits $17 < m_I < 19$ and $1.2 < V - I < 3.5$ following Gazak et al. (2015). The lower limit of this box are naturally blended in to a population of super-AGB stars which can have luminosities comparable to the faintest RSGs (Nikolaev & Weinberg, 2000, e.g.). However, as stated in Chapter ?? these stars are known to have lifetimes similar to the lowest mass RSGs and arguably still trace the young stellar population of this galaxy.

Table 1.2 shows ground- and space-based optical photometry of the KMOS targets along with their radial velocities (see section 1.5.1).

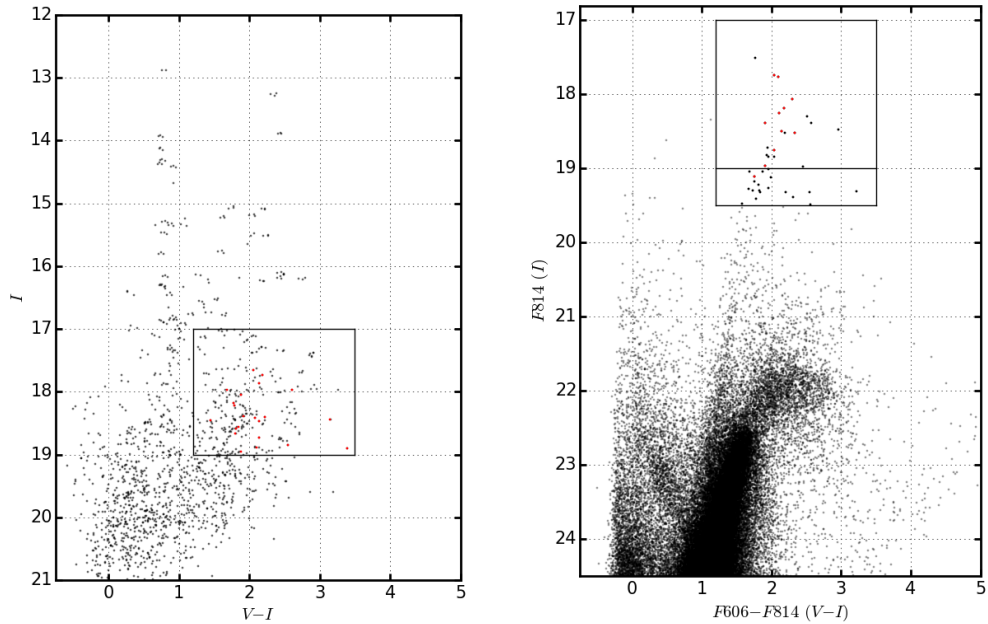


Figure 1.3 *NGC 55 ground- and space-based $V - I$ against I CMDs.* Left hand panel shows data from the ground-based Araucaria Project Gieren et al. (2005) over the entire FoV of the KMOS observations. Right hand panel shows data from the ANGST project (blue; ANGST Dalcanton et al., 2009) where photometry from this project covers only a portion of the KMOS FoV. The black boxes in each panel define candidate RSGs, which are defined as $17 < F814 < 19$ and $1.2 < F606 - F814 < 3.5$ in the right hand panel and consequently applied to a larger FoV in the left hand panel assuming a one-to-one relationship between the ground- and space-based filters.

Table 1.2 Summary of VLT-KMOS targets in NGC 55.

ID	S/N	α (J2000)	δ (J2000)	V ^a	I ^a	F606 ^b	F814 ^b	$\langle rv \rangle$ (km s ⁻¹)			Notes
								14-09-2013	16-10-2013	14-09-2014	
NGC55-RSG19	xx	00:15:29.190	-39:14:08.20	19.914	17.731	19.85	17.76	205±4	178±7	191±7	199±14
NGC55-RSG20	xx	00:15:29.520	-39:15:13.00	20.832	18.952	20.86	19.11	194±14	220±5	-	217±10
NGC55-RSG22	xx	00:15:30.520	-39:16:36.70	20.406	18.589	-	18.38	95±14	-41±26	-	Notes
NGC55-RSG24	xx	00:15:31.460	-39:14:46.30	20.612	18.475	20.29	18.38	186±6	194±7	146±38	192±16
NGC55-RSG25	xx	00:15:31.490	-39:14:32.40	20.316	18.394	20.63	18.49	204±12	217±16	-376±41 ^c	151±23
NGC55-RSG26	xx	00:15:33.160	-39:13:42.00	20.572	17.964	20.35	18.06	174±9	173±8	-	200±26
NGC55-RSG28	xx	00:15:36.160	-39:15:29.40	21.001	18.892	20.87	18.97	233±17	161±20	-	173±1
NGC55-RSG30	xx	00:15:38.030	-39:14:50.20	20.867	18.730	20.79	18.75	212±10	215±10	-424±21 ^c	203±41
NGC55-RSG35	xx	00:15:39.260	-39:15:01.70	20.007	17.872	19.78	17.73	202±3	206±4	223±13	213±2
NGC55-RSG36	xx	00:15:39.520	-39:16:23.10	19.915	18.462	-	-	-188±31	-284±16	-588±35	204±5
NGC55-RSG39	xx	00:15:40.260	-39:15:01.00	19.654	17.970	20.36	18.19	206±11	192±5	-1±30 ^c	-
NGC55-RSG43	xx	00:15:40.700	-39:14:50.20	19.957	18.183	20.36	18.25	-220±20 ^c	196±5	173±17	193±14
NGC55-RSG46	xx	00:15:41.640	-39:14:58.80	21.591	18.441	20.85	18.52	228±5	195±6	-128±18 ^c	194±9
NGC55-RSG57	xx	00:15:45.590	-39:15:16.40	20.010	18.220	-	-	217±10	197±6	207±13	214±18
NGC55-RSG58	xx	00:15:46.270	-39:15:43.20	20.619	18.400	-	-	236±8	216±3	214±21	193±16
NGC55-RSG60	xx	00:15:49.180	-39:17:19.80	21.393	18.847	-	-	-73±39	26±26	-533±39	218±8
NGC55-RSG65	xx	00:15:51.250	-39:16:26.40	19.706	17.653	-	-	224±5	215±4	94±37	-
NGC55-RSG67	xx	00:15:53.110	-39:14:13.60	19.925	18.047	-	-	25±24 ^c	217±6	210±8	Notes
NGC55-RSG69	xx	00:15:55.280	-39:15:00.10	20.470	18.666	-	-	231±5	195±9	177±6	Notes
NGC55-RSG70	xx	00:15:56.310	-39:16:08.60	22.300	18.907	-	-	155±12	187±9	210±13	Notes
NGC55-RSG71	xx	00:15:56.900	-39:15:27.50	20.401	18.559	-	-	197±11	214±11	202±20	180±20
NGC55-RSG73	xx	00:15:57.710	-39:15:41.50	20.489	18.411	-	-	161±7	178±6	320±16 ^c	206±12
								136±35	136±35	-476±42 ^c	Notes
										176±19	171±11

^a Ground based data from the Araucaria Project Pietrzynski et al. (2006), with typical photometric uncertainty 0.075 and 0.016 in V and I bands respectively.

^b HST ANGST photometry from Dalcanton et al. (2009), with typical errors 0.12, 0.13 in F606 and F814 bands respectively.

^c Value excluded from average for target.

1.4 Data Reduction

The data reduction was performed with the KMOS/esorex pipeline with a several corrections to improve the quality of the reductions which are fully described and characterised in Turner et al. (in prep).

- Split recombined sky frames into seeing bins
- combine by including pixel shifts between reconstructed IFUs to ensure all frames are correctly matched
- etc.

Would it be useful to use Skycorr to subtract the sky as in Gazak et al. (2015)

Telluric correction has been performed by combining and reconstructing the telluric standard exposures using the standard pipeline routines. To improve the performance of the telluric correction I use the method described in detail in Chapter ??.

As mentioned above, were multiple standard star OBs for each night of observing. The telluric spectrum used to correct each science spectrum is determined on a star-by-star basis depending upon a visual inspection of the results of the correction.

1.5 Results

1.5.1 Radial Velocities

Radial velocities are measured using the method described first in Chapter ?? where radial velocities are measured using several strong spectral features within the $1.16\text{--}1.21\mu\text{m}$ region. Each of these spectral features is independently used to measure a radial velocity where the value quoted is the average of these measurements and the uncertainties are defined by the standard deviation of the measurements. This method is known to work well on KMOS stellar spectra Lapenna et al. (2015); Patrick et al. (2015, 2016).

Estimated radial velocities from each KMOS pointing is listed in Table 1.2 alongside the average radial velocity for each target, where any significantly discrepant measurement has been excluded (marked by note c in Table 1.2). Uncertainties quoted on the average are the standard deviation of the measurements on each night. Three targets (NGC55-RSG22, NGC55-RSG36 and NGC55-RSG60) have been excluded from this average based on their unreliable radial velocity estimates. Given the significant variability in these measurements on each night, an assessment on membership to NGC 55 is impossible given the current data.

Comparing the estimated velocities to previous measurements we find good agreement with velocities measured for ~ 200 BSGs in NGC 55 in (Castro et al., 2008) as well as with measurements of the velocity from the HI gas (Puche, Carignan & Wainscoat, 1991). The estimated radial velocities as a function of galactocentric distance is shown in Figure 1.4 where previous measurements are also shown for comparison. The radius at which the surface brightness first reach 25 mag/arcsec² in the *B*-band (R_{25} e.g. ?) is shown for scale ($R_{25} = 16.2 \pm 0.4$ arcmin de Vaucouleurs et al., 1991) We find no evidence for a systematic offset between the measurements of Castro et al. (2008) and those measured in this study.

As the observed data is taken over four different epochs, the variability of each source can be assessed. No clear evidence for variability is found for any target within the observed sample. To assess variability the variability criteria of (?) is employed, i.e.

$$\left| \frac{RV_i - \mu}{\sigma_i} \right| > 4.0, \quad (1.1)$$

where RV_i is the radial velocity with an associated uncertainty σ_i measured on an individual night i and μ is the average radial velocity for the target. Using this criteria on all targets finds that no targets show evidence for variability.

1.5.2 Stellar Parameters

- Comparison to previous results Castro et al. (2012) find average $[Z] = -0.4 \pm 0.13$ dex Z Vs. Radius from galaxy centre

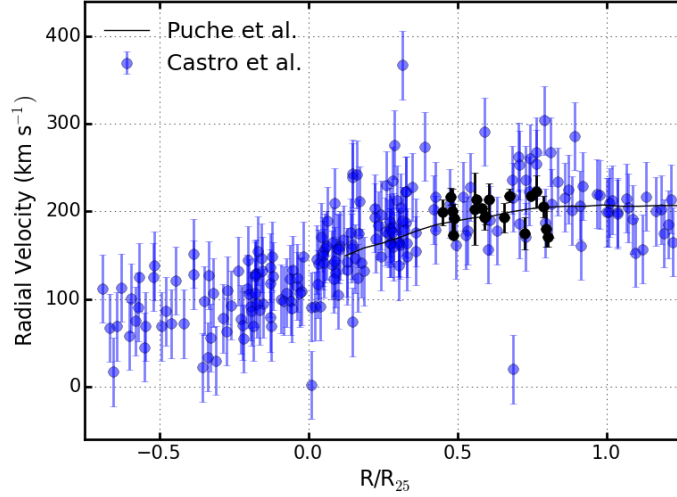


Figure 1.4 Radial velocities for the KMOS RSGs (black points) shown against projected radius from the centre of NGC 55 as defined by the Two Micron All Sky Survey (2MASS; Skrutskie et al., 2006) scaled by $R_{25} = 16.2 \pm 0.4$ arcmin (de Vaucouleurs et al., 1991). Blue points show data for ~ 200 BSGs in NGC 55 from (Castro et al., 2008, ; shown with 50% transparency to highlight densely populated areas) alongside the rotation curve of NGC 55 (black solid line; Puche, Carignan & Wainscoat, 1991).

- MCMC parameter estimation for the fit
- Extinction values need to be taken into account (especially if I'm estimating luminosities in the I band)

Distance modulus = 26.58 ± 0.11 (Tanaka et al., 2011). Distance modulus = 26.434 ± 0.037 (Gieren et al., 2008)

1.6 Discussion

- Orientation of NGC 55

1.7 Conclusions

Bibliography

- Castro N. et al., 2008, A&A, 485, 41
- Castro N. et al., 2012, A&A, 542, A79
- Dalcanton J. J. et al., 2009, ApJS, 183, 67
- Davidge T. J., 2005, ApJ, 622, 279
- de Vaucouleurs G., 1961, ApJ, 133, 405
- de Vaucouleurs G., de Vaucouleurs A., Corwin, Jr. H. G., Buta R. J., Paturel G., Fouqué P., 1991, Third Reference Catalogue of Bright Galaxies. Volume I: Explanations and references. Volume II: Data for galaxies between 0^h and 12^h . Volume III: Data for galaxies between 12^h and 24^h .
- Engelbracht C. W. et al., 2004, ApJS, 154, 248
- Ferguson A. M. N., Wyse R. F. G., Gallagher J. S., 1996, AJ, 112, 2567
- Gazak J. Z. et al., 2015, ApJ, 805, 182
- Gieren W. et al., 2005, The Messenger, 121, 23
- Gieren W., Pietrzyński G., Soszyński I., Bresolin F., Kudritzki R.-P., Storm J., Minniti D., 2008, ApJ, 672, 266
- Houk N., 1978, Michigan catalogue of two-dimensional spectral types for the HD stars
- Houk N., Smith-Moore M., 1988, Michigan Catalogue of Two-dimensional Spectral Types for the HD Stars. Volume 4, Declinations $-26^{\circ}0' - 12^{\circ}0'$.
- Hummel E., Dettmar R.-J., Wielebinski R., 1986, A&A, 166, 97

- Karachentsev I. D. et al., 2003, A&A, 404, 93
- Koribalski B. S. et al., 2004, AJ, 128, 16
- Lapenna E., Origlia L., Mucciarelli A., Lanzoni B., Ferraro F. R., Dalessandro E., Valenti E., Cirasuolo M., 2015, ApJ, 798, 23
- Nikolaev S., Weinberg M. D., 2000, ApJ, 542, 804
- Patrick L. R., Evans C. J., Davies B., Kudritzki R., Hénault-Brunet V., Bastian N., Lapenna E., Bergemann M., 2016, ArXiv e-prints
- Patrick L. R., Evans C. J., Davies B., Kudritzki R.-P., Gazak J. Z., Bergemann M., Plez B., Ferguson A. M. N., 2015, ApJ, 803, 14
- Pietrzynski G. et al., 2006, AJ, 132, 2556
- Pritchett C. J., Schade D., Richer H. B., Crabtree D., Yee H. K. C., 1987, ApJ, 323, 79
- Puche D., Carignan C., Wainscoat R. J., 1991, AJ, 101, 447
- Robinson B. J., van Damme K. J., 1964, in IAU Symposium, Vol. 20, The Galaxy and the Magellanic Clouds, Kerr F. J., ed., p. 276
- Skrutskie M. F. et al., 2006, AJ, 131, 1163
- Tanaka M., Chiba M., Komiyama Y., Guhathakurta P., Kalirai J. S., 2011, ApJ, 738, 150
- van de Steene G. C., Jacoby G. H., Praet C., Ciardullo R., Dejonghe H., 2006, A&A, 455, 891
- Webster B. L., Smith M. G., 1983, MNRAS, 204, 743
- Westmeier T., Koribalski B. S., Braun R., 2013, MNRAS, 434, 3511

Chapter 2

Conclusions and Future Work

Bibliography

- Castro N. et al., 2008, A&A, 485, 41
- Castro N. et al., 2012, A&A, 542, A79
- Dalcanton J. J. et al., 2009, ApJS, 183, 67
- Davidge T. J., 2005, ApJ, 622, 279
- de Vaucouleurs G., 1961, ApJ, 133, 405
- de Vaucouleurs G., de Vaucouleurs A., Corwin, Jr. H. G., Buta R. J., Paturel G., Fouqué P., 1991, Third Reference Catalogue of Bright Galaxies. Volume I: Explanations and references. Volume II: Data for galaxies between 0^h and 12^h . Volume III: Data for galaxies between 12^h and 24^h .
- Engelbracht C. W. et al., 2004, ApJS, 154, 248
- Ferguson A. M. N., Wyse R. F. G., Gallagher J. S., 1996, AJ, 112, 2567
- Gazak J. Z. et al., 2015, ApJ, 805, 182
- Gieren W. et al., 2005, The Messenger, 121, 23
- Gieren W., Pietrzyński G., Soszyński I., Bresolin F., Kudritzki R.-P., Storm J., Minniti D., 2008, ApJ, 672, 266
- Houk N., 1978, Michigan catalogue of two-dimensional spectral types for the HD stars
- Houk N., Smith-Moore M., 1988, Michigan Catalogue of Two-dimensional Spectral Types for the HD Stars. Volume 4, Declinations -26deg.0 to -12deg.0.
- Hummel E., Dettmar R.-J., Wielebinski R., 1986, A&A, 166, 97
- Karachentsev I. D. et al., 2003, A&A, 404, 93
- Koribalski B. S. et al., 2004, AJ, 128, 16
- Lapenna E., Origlia L., Mucciarelli A., Lanzoni B., Ferraro F. R., Dalessandro E., Valenti E., Cirasuolo M., 2015, ApJ, 798, 23

- Nikolaev S., Weinberg M. D., 2000, ApJ, 542, 804
- Patrick L. R., Evans C. J., Davies B., Kudritzki R., Hénault-Brunet V., Bastian N., Lapenna E., Bergemann M., 2016, ArXiv e-prints
- Patrick L. R., Evans C. J., Davies B., Kudritzki R.-P., Gazak J. Z., Bergemann M., Plez B., Ferguson A. M. N., 2015, ApJ, 803, 14
- Pietrzynski G. et al., 2006, AJ, 132, 2556
- Pritchett C. J., Schade D., Richer H. B., Crabtree D., Yee H. K. C., 1987, ApJ, 323, 79
- Puche D., Carignan C., Wainscoat R. J., 1991, AJ, 101, 447
- Robinson B. J., van Damme K. J., 1964, in IAU Symposium, Vol. 20, The Galaxy and the Magellanic Clouds, Kerr F. J., ed., p. 276
- Skrutskie M. F. et al., 2006, AJ, 131, 1163
- Tanaka M., Chiba M., Komiyama Y., Guhathakurta P., Kalirai J. S., 2011, ApJ, 738, 150
- van de Steene G. C., Jacoby G. H., Praet C., Ciardullo R., Dejonghe H., 2006, A&A, 455, 891
- Webster B. L., Smith M. G., 1983, MNRAS, 204, 743
- Westmeier T., Koribalski B. S., Braun R., 2013, MNRAS, 434, 3511